Multi-AUV Control and Adaptive Sampling in Monterey Bay

Edward Fiorelli, *Member, IEEE*, Naomi Ehrich Leonard, *Senior Member, IEEE*, Pradeep Bhatta, *Member, IEEE*, Derek A. Paley, *Student Member, IEEE*, Ralf Bachmayer, *Member, IEEE*, and David M. Fratantoni, *Member, IEEE*

***Abstract*—Operations with multiple autonomous underwater vehicles (AUVs) have a variety of underwater applications. For example, a coordinated group of vehicles with environmental sensors can perform adaptive ocean sampling at the appropriate spatial and temporal scales. We describe a methodology for cooperative control of multiple vehicles based on virtual bodies and artificial potentials (VBAP). This methodology allows for adaptable formation control and can be used for missions such as gradient climbing and feature tracking in an uncertain environment. We discuss our implementation on a fleet of autonomous underwater gliders and present results from sea trials in Monterey Bay in August, 2003. These at-sea demonstrations were performed as part of the Autonomous Ocean Sampling Network (AOSN) II project.**

***Index Terms*—Adaptive sampling, autonomous underwater vehicles (AUVs), cooperative control, formations, gradient climbing, underwater gliders.**

I. Introduction

COORDINATED groups of autonomous underwater vehicles (AUVs) can provide significant benefit to a number of applications including ocean sampling, mapping, surveillance, and communication [1]. With the increasing feasibility and decreasing expense of the enabling vehicle, sensor, and communication technologies, interest in these compelling applications is growing and multi-AUV operations are beginning to be realized in the water. Indeed, we report here on results of our tests of multi-AUV cooperative control of a fleet of autonomous underwater gliders in Monterey Bay, CA, in August, 2003.

In many multiple vehicle tasks, it is critical to determine the relevant spatial and temporal scales. For instance, in the case that the AUV group is to function as a communication network, the spatial scale may be determined by the communication range. In certain ocean sensing applications, the temporal scale may be driven by the dynamics of the ocean process of interest. The spatial and temporal scales central to the mission provide a useful way to classify multivehicle tasks and the associated vehicle, communication, control, and coordination requirements and relevant methodologies.

When each vehicle is equipped with sensors for observing its environment, the group may serve as a mobile sensor network. In the case that a mobile sensor network is to be used to sample the physical and/or biological variables in the water, the range of relevant spatial and temporal scales can be dramatic. Sampling in a relatively large area may be of interest to observe large-scale processes (e.g., upwelling and relaxation) and to understand the influence of external forcing. We refer to the sampling problem for the larger scales as the *broad-area coverage* problem. As a complement, *feature tracking* addresses the problem of measuring more local phenomena such as fronts, plumes, eddies, and algae blooms.

From one end to the other of the spectrum of scales, multiple AUVs and cooperative control have much to contribute. However, requirements and strategies will differ. For example, vehicle endurance will be critical for broad-area coverage while vehicle speed may be of particular interest for feature tracking. While vehicle-to-vehicle communication may be impractical for broad-area coverage, it may be feasible for feature tracking. At both ends of the spatial scale spectrum, feedback control and coordination can be central to the effective behavior of the collective. However, the most useful vehicle paths may be different at different scales, e.g., vehicle formations for small scales and coordinated but separated trajectories for large scales.

There is a large and growing literature on cooperative control in control theory, robotics, and biology. For a survey with representation from each of these communities see [2]. There are fewer examples of full-scale, cooperative multi-AUV demonstrations in the water. One example by Schultz *et al.* is described in [3].

In this paper, we describe cooperative control and adaptive sampling strategies and present results from sea trials with a fleet of autonomous underwater gliders in Monterey Bay during August, 2003. These sea trials were performed as part of the Autonomous Ocean Sampling Network (AOSN) II project [4]. A central objective of the project is to bring robotic vehicles together with ocean models to improve our ability to observe and predict ocean processes. New cooperative control and adaptive sampling activities are underway as part of the Adaptive Sampling and Prediction (ASAP) project [5]. Sea trials for this project will take place in Monterey Bay in 2006.

Manuscript received June 30, 2005; revised February 5, 2006; accepted March 1, 2006. This work was supported in part by the Office of Naval Research under Grants N00014-02-1-0826 and N00014-02-1-0861, by the National Science Foundation under Grant CCR-9980058, by the Air Force Office of Scientific Research under Grant F49620-01-1-0382, and by the Pew Charitable Trust under Grant 2000-002558. **Guest and Associate Editors: H. Singh, C. Brancart, and J. F. Lynch**.

E. Fiorelli was with the Mechanical and Aerospace Engineering, Princeton University, Princeton, NJ 08544 USA. He is now with the Remote Sensing and Surveillance Group, Northrop Grumman, Azusa, CA 91702 USA (e-mail: Edward.Fiorelli@ngc.com).

N. E. Leonard and D. A. Paley are with the Mechanical and Aerospace Engineering, Princeton University, Princeton, NJ 08544 USA (e-mail: naomi@princeton.edu; dpaley@princeton.edu).

P. Bhatta is with the Princeton Satellite Systems, Inc., Princeton, NJ 08540 USA (e-mail: pradeep@psatellite.com).

R. Bachmayer is with the National Research Council Institute for Ocean Technology, St. John's, NL A1B 3T5, Canada (e-mail: Ralf.Bachmayer@nrc.ca).

D. M. Fratantoni is with the Physical Oceanography Department, Woods Hole Oceanographic Institution, Woods Hole, MA 02543 USA (e-mail: dfratantoni@whoi.edu).

Digital Object Identifier 10.1109/JOE.2006.880429

In Section II, we summarize our cooperative control strategy based on *virtual bodies and artificial potentials* (VBAP) and discuss its application to feature tracking. VBAP is a general strategy for coordinating the translation, rotation, and dilation of an array of vehicles so that it can perform a mission such as climbing a gradient in an environmental field. Artificial potentials play an important role in this construction. In robotics, they have been extensively used to produce feedback control laws [6]–[9] for avoidance of stationary obstacles as well as obstacles in motion [10] and have been used in motion planning [11]. In an oceanographic application, they were used in [12] in a depth following algorithm for the autonomous benthic explorer (ABE) vehicle.

The challenges and solutions to implementing VBAP on a glider fleet in Monterey Bay are described in Section III. Results from the Monterey Bay 2003 sea trials are described and analyzed in Section IV. As part of this analysis, we evaluate one of the coordinated multivehicle demonstrations for the influence of the sampling patterns on the quality of the data set using a metric based on objective analysis mapping error [13]. In Section V, we describe how, in work in progress, we use this metric to approach optimal design of mobile sensor arrays for broad-area coverage.

II. Cooperative Control: VBAP

In this section, we present a brief overview of VBAP multivehicle control methodology. This methodology provides adaptable formation control and is well-suited to multivehicle applications, such as feature tracking, in which regular formations are of interest. For example, the methodology can be used to enable mobile sensor arrays to perform adaptive gradient climbing of a sampled environmental field. The general theory for adaptable formation control and adaptive gradient climbing is presented in [14]–[16] and specialization to a fleet of underwater gliders in [16] and [17].

VBAP relies on artificial potentials and virtual bodies to coordinate a group of vehicles modeled as point masses (with unit mass) in a provably stable manner. The virtual body consists of linked, moving reference points called *virtual leaders*. Artificial potentials are imposed to couple the dynamics of vehicles and the virtual body. These artificial potentials are designed to create desired vehicle-to-vehicle spacing and vehicle-to-virtual-leader spacing. Potentials can also be designed for desired orientation of vehicle position relative to virtual leader position. With these potentials, a range of vehicle group shapes can be produced [16], [18]. The approach brings the group of vehicles into formation about the virtual body as the virtual body moves. The artificial potentials are realized by means of the vehicle control actuation: The control law for each vehicle is derived from the gradient of the artificial potentials.

The dynamics of the virtual body can also be prescribed as part of the multivehicle control design problem. The methodology allows the virtual body, and thus the vehicle group, to perform maneuvers that include translation, rotation, and contraction/expansion, all the while ensuring that the formation error remains bounded. In the case that the vehicles are equipped with sensors to measure the environment, the maneuvers can be driven by measurement-based estimates of the environment. This permits the vehicle group to perform as an adaptable sensor array.

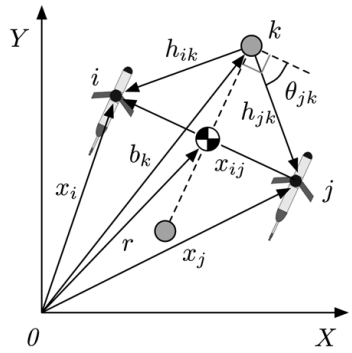

Fig. 1. Notation for framework. Shaded circles are virtual leaders.

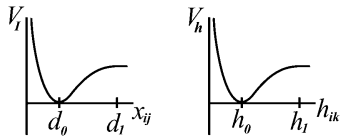

Fig. 2. Representative artificial potentials V_I and V_h.

VBAP is designed for vehicles moving in three-dimensional (3-D) space $\mathbb{R}^3$; for simplicity of presentation, we summarize the case in two-dimensional (2-D) space $\mathbb{R}^2$. Let the position of the ith vehicle in a group of N vehicles, with respect to an inertial frame, be given by a vector $x_i \in \mathbb{R}^2$, $i = 1, \ldots, N$ as shown in Fig. 1. The position of the kth virtual leader with respect to the inertial frame is $b_k \in \mathbb{R}^2$, for $k = 1, \ldots, M$. The position vector from the origin of the inertial frame to the center of mass of the virtual body is given by $r = (1/M) \sum_{k=1}^{M} b_k \in \mathbb{R}^2$. Let $x_{ij} = x_i - x_j \in \mathbb{R}^2$ and $h_{ik} = x_i - b_k \in \mathbb{R}^2$. The control force on the ith vehicle is given by $u_i \in \mathbb{R}^2$. Assuming full actuation, the dynamics can be written for $i = 1, \ldots, N$ as

$$\ddot{x}_i = u_i.$$

We define the state of the vehicle group as $x = (x_1, \ldots, x_N, \dot{x}_1, \ldots, \dot{x}_N)$.

Between every pair of vehicles i and j we define an artificial potential $V_I(x_{ij})$ and between every vehicle i and every virtual leader k we define an artificial potential $V_h(h_{ik})$. An additional potential $V_r(\theta_{ik})$ can be used to orient the angles $\theta_{ik} = \arg h_{ik}$. The control law for the ith vehicle, u_i is defined as minus the gradient of the sum of these potentials

$$u_i = -\sum_{j \neq i}^{N} \nabla_{x_i} V_I(x_{ij}) - \sum_{k=1}^{M} \left(\nabla_{x_i} V_h(h_{ik}) + \nabla_{x_i} V_r(\theta_{ik}) \right).$$

A typical form for V_I and V_h is shown in Fig. 2. Note that in this example, V_I yields a force that is repelling when a pair of vehicles is too close, i.e., when $||x_{ij}|| < d_0$, attracting when the vehicles are too far, i.e., when $||x_{ij}|| > d_0$ and zero when the vehicles are very far apart $||x_{ij}|| \geq d_1 > d_0$ or when $||x_{ij}|| = d_0$, where d_0 and d_1 are constant design parameters. The potential $V_r(\theta_{ik})$ is designed so that it has isolated global minima at specified angles about the virtual leader; examples are presented in [16] and [17].

In [18], local asymptotic stability of $x = x_{eq}$ corresponding to the vehicles at rest at the global minimum of the sum of the artificial potentials is proved with the Lyapunov function

$$\Phi(x) = \frac{1}{2}\sum_{i=1}^{N}\left[\|\dot{x}_i\|^2 + \sum_{j\neq i}^{N} V_I(x_{ij}) + 2\sum_{k=1}^{M}\left(V_h(h_{ik}) + V_r(\theta_{ik})\right)\right]. \quad (1)$$

This Lyapunov function also serves as a formation *error function* in what is to follow. We assume the artificial potentials are designed so that $\Phi \geq 0$.

To achieve formation maneuvers, dynamics are designed for the virtual body. The configuration of the virtual body is defined by its position vector r, its orientation $R \in SO(2)$ (the 2×2 rotation matrix parameterized by the angle of rotation in the plane), and its scalar dilation factor κ which determines the magnitude of expansion or contraction. An M-vector ϕ can also be defined to fix additional degrees of freedom in the formation shape using V_r. The design problem is to choose expressions for the dynamics dr/dt, dR/dt, $d\kappa/dt$, and $d\phi/dt$.

As a means to design the virtual body dynamics to ensure stability of the formation during a mission from time t_0 to t_f, the path of the virtual body in configuration space is parameterized by a scalar variable s, i.e., $r(s)$, $R(s)$, $\kappa(s)$, and $\phi(s)$ for $s \in [s_s, s_f]$, where $s_s = s(t_0)$ and $s_f = s(t_f)$. Then, the virtual body dynamics can be written as

$$\frac{dr}{dt} = \frac{dr}{ds}\dot{s} \quad \frac{dR}{dt} = \frac{dR}{ds}\dot{s} \quad \frac{d\kappa}{dt} = \frac{d\kappa}{ds}\dot{s} \quad \frac{d\phi}{dt} = \frac{d\phi}{ds}\dot{s}$$

where $\dot{s} = ds/dt$. The formation error defined by (1) becomes $\Phi(x, s)$ because the configuration of the virtual body, and, therefore, the artificial potentials are a function of s.

The speed along the path $\dot{s}$ is chosen as a function of the formation error to guarantee stability and convergence of the formation. The idea is that the virtual body should slow down if the formation error grows too large and should maintain a desired nominal speed if the formation error is small. Given a user-specified, scalar upper bound on the formation error Φ_U and a desired nominal group speed v_0, boundedness of the formation error and convergence to the desired formation is proven [14] with the choice

$$\dot{s} = h(\Phi(x,s)) - \frac{\left(\frac{\partial\Phi}{\partial x}\right)^T \dot{x}}{\delta + \left|\frac{\partial\Phi}{\partial s}\right|}\left(\frac{\delta + \Phi_U}{\delta + \Phi(x,s)}\right) \quad (2)$$

with initial condition $s(t_0) = s_s$, $\delta \ll 1$ a small parameter, and

$$h(\Phi) = \begin{cases} \frac{1}{2}v_0\left(1 + \cos\left(\pi\frac{2}{\Phi_U}\Phi\right)\right), & \text{if } \Phi \leq \frac{\Phi_U}{2} \\ 0, & \text{if } \Phi > \frac{\Phi_U}{2} \end{cases}.$$

$\dot{s}$ is set to zero when $s \geq s_f$. Notation $(\cdot)^T$ denotes matrix transpose.

The remaining freedom in the direction of the virtual body dynamics, i.e., dr/ds, dR/ds, $d\kappa/ds$, and $d\phi/ds$, can be assigned to satisfy the mission requirements of the group. For example, the choice

$$\frac{dr}{ds} = \begin{pmatrix} 1 \\ 0 \end{pmatrix} \quad \frac{dR}{ds} = 0 \quad \frac{d\kappa}{ds} = 1$$

produces a formation that expands in time with its center of mass moving in a straight line in the horizontal direction and its orientation fixed. Stability and convergence of the formation are guaranteed by the choice of $\dot{s}$, independent of the choice of group mission.

As another possibility, the specification of virtual body direction can be made as a feedback function of measurements taken by sensors on the vehicles. For instance, suppose that each vehicle can measure a scalar environmental field T such as temperature or salinity or biomass concentration. These measurements can be used to estimate the gradient of the field ∇T_{est} at the center of mass of the group. If the mission is to move the vehicle group to a maximum in the field T, e.g., warm regions or high-concentration areas, an appropriate choice of direction is

$$\frac{dr}{ds} = \nabla T_{\text{est}}.$$

This drives the virtual body, and thus the vehicle group, to a local maximum in T. Convergence results for gradient climbing using least-squares estimation of gradients (with the option of Kalman filtering to use past measurements) are presented in [14]. The optimal formation (shape and size) that minimizes the least-square gradient estimation error is also investigated. Adaptive gradient climbing is possible; for example, the dilation of the formation (resolution of the sensor array) can be changed for optimal estimation of the field in response to measurements.

The approach to gradient climbing can be extended to drive formations to and along fronts and boundaries of features. For example, in [16] measurements of a scalar field are used to compute second and higher order derivatives in the field, necessary for estimating front locations (e.g., locations of maximum gradient). In [19], tracking of level sets is achieved using curvature estimates.

III. Cooperative Control of Autonomous Underwater Glider Fleets

The theory summarized in Section II does not directly address various operational constraints and realities associated with real vehicles in the water. In this section, we address a number of these issues in a summary of our implementation of the VBAP methodology for a fleet of underwater gliders in Monterey Bay. For example, the control laws are modified to accommodate constant speed constraints consistent with glider motion and to cope with external currents. The implementation also treats underwater gliders that were configured to track waypoints and to communicate infrequently. In this paper, we provide an overview of the implementation; more details can be found in [16] and [17].

In August, 2003, we performed sea trials with a fleet of Slocum autonomous gliders as part of the AOSN II project. Gliders were controlled in formations using the VBAP method-

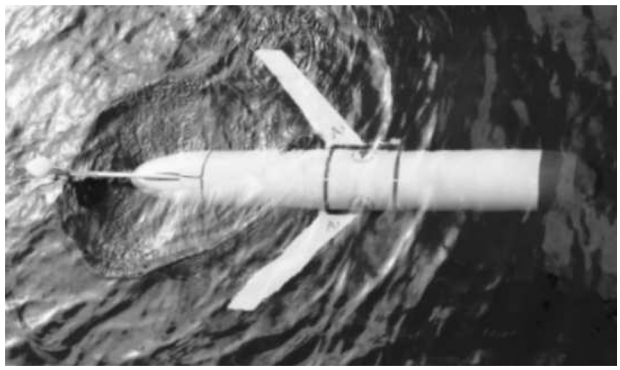

Fig. 3. Slocum glider manufactured by Webb Research Corporation and operated by D. M. Fratantoni.

ology with implementation as described here. Sea-trial results are described in Section IV. In these sea trials, the currents were challenging in the many ways described later; however, on the whole, the methodology, with the modifications described in this section, was successful.

A. Autonomous Underwater Glider

Autonomous underwater gliders are a class of energy-efficient AUVs designed for continuous, long-term deployment [20]. Due to their relative low cost and high endurance, gliders are particularly well suited for deployment in large numbers. Consequently, gliders are playing an increasingly critical role in autonomous, large-scale ocean surveys [4]. Over the last few years, three types of ocean going underwater gliders have been developed for oceanographic applications: the Slocum [21], the Spray [22], and the Seaglider [23]. A Slocum glider operated by D. M. Fratantoni and manufactured by Webb Research Corporation (East Falmouth, MA) is shown in Fig. 3.

The energy efficiency of the gliders is due in part to the use of a buoyancy engine. Gliders control their net buoyancy to change their vertical direction of motion. Actively controlled redistribution of internal mass is used to adjust pitch and/or roll, although the Slocum uses a rudder for heading control. Fixed wings provide lift which induces motion in the horizontal direction. The nominal motion of the glider in the longitudinal plane is along a sawtooth trajectory where one down–up cycle is called a *yo*. Having no active thrust elements, glider trajectories are easily perturbed by external currents. The effective horizontal speed of the Slocum gliders is less than 40 cm/s.

The Slocum glider is equipped with an Iridium-based, global communication system and a line-of-sight, high-bandwidth Freewave system for data communication. Neither system, however, can be operated underwater.

The Slocum glider operates autonomously, tracking waypoints or setpoints in the horizontal plane. While underwater, the glider uses dead reckoning for navigation, computing its position using its pressure sensor, attitude measurement, and integration of its horizontal-plane speed estimate.

Gliders are inherently sensitive to ocean currents and the Slocum includes the effects of external currents in its dead reckoning algorithms and heading controller. However, during a dive cycle, the glider does not have a local current measurement. Instead, the glider uses a constant estimate computed at the last surfacing by comparing dead-reckoned position with recently acquired global positioning system (GPS) fixes. Any error between the two is attributed to an external current. This information is also made available as science data.

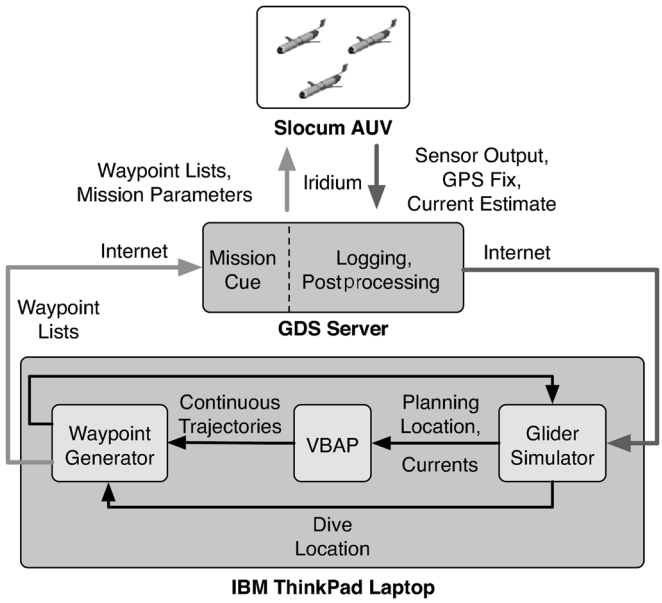

Fig. 4. AOSN II VBAP-glider system operational configuration and data-flow diagram.

Gliders can be equipped with a variety of sensors for gathering data useful for oceanographers and ocean modelers. The Slocum gliders used in Monterey Bay in 2003 housed sensors for temperature, salinity, depth, chlorophyll fluorescence, optical backscatter, and photosynthetic active radiation (PAR). Sensor measurements can be used to drive multivehicle feedback control algorithms with the goal of collecting data that is most useful to understanding the environment. This contributes to what is known as *adaptive sampling*, discussed in Section III-D.

B. Implementation of VBAP for a Network of Gliders

As part of the AOSN II experiment during August, 2003, up to 12 Slocum gliders, operated by author D. M. Fratantoni, were deployed in Monterey Bay. The Slocum gliders were monitored from the central shore station located at the Monterey Bay Aquarium Research Institute (MBARI) at Moss Landing, CA. Every time a glider surfaced, it communicated via Iridium with the glider data system (GDS) at the Woods Hole Oceanographic Institution (WHOI) in Woods Hole, MA. The GDS is a custom software suite that provides real-time monitoring and mission cuing services for multiple-Slocum glider operations. New missions were uploaded to the GDS from MBARI through the internet. Likewise, glider data was downloaded from the GDS to MBARI through the internet. During 2003, each of the gliders surfaced (independently) every 2 h. No underwater communication between gliders was available.

To coordinate fleets of underwater gliders, we applied the general control theory of Section II to the seafaring glider AUVs. Fig. 4 presents a schematic view of the coupled VBAP-glider system implemented during AOSN II.

In this implementation, waypoint lists generated from the VBAP output are transmitted to the gliders via the GDS interface. When a glider surfaces it attempts to acquire a quality GPS fix and then establishes an Iridium connection with the GDS server at WHOI. The recently acquired GPS fix (if available), sensor profile data, and estimated external currents are uploaded to the GDS server for quality control and logging. At any time, the option exists to halt the current mission plan and upload a new one. A mission plan consists of a set of waypoints specified in the horizontal plane, yo depth bounds, and maximum duration. During the coordinated control demonstrations in 2003, we ran VBAP on an onshore computer to determine a new mission plan once every 2 h for all the gliders included in the demonstration. To limit the time spent on the surface by the gliders, mission plans for each glider were available immediately at surfacing. Thus, the latest information was not used for design of the immediate mission plan.

To provide mission plans to each glider upon surfacing, an estimate is needed of the dive location of each glider at the start of its next mission, denoted *dive location*. Also needed for each glider is its location when the *lead* glider dives, denoted *planning location*. The lead glider is the glider that surfaces first in each surfacing of the group. Since we could call any of the gliders the first in the group, we make the choice that minimizes the time from the first to the last glider surfacing.

Waypoints from VBAP output are generated for all gliders simultaneously. The planning locations are used in initializing VBAP. The dive locations are used to ensure the waypoint lists to be generated are consistent with the locations of the other gliders when they actually start the mission. Both sets of locations are necessary because of surfacing asynchronicities among gliders in the formation.

Both planning and diving locations are generated by a *glider simulator* which is a dynamic simulation using a simple model of the Slocum glider. As inputs, the glider simulator utilizes the current mission plan, last known position before diving, and the currents reported during the last mission. An in-depth discussion of the simulator can be found in [16] and [17].

VBAP is initialized with the estimated planning location for each glider and the average of the last reported estimated currents. VBAP is then run ahead for planning purposes on simulated glider dynamics that include this average current. The continuous trajectories generated by VBAP are discretized into waypoints in the *waypoint generator*. The discretization is performed using constrained minimization of an appropriate cost function [16], [17]. In the process of generating waypoints, we ensure that the new mission waypoints are compatible with the dive locations to avoid unnecessary backtracking. In particular, if the output of the waypoint generator is expected to yield backtracking, we have the option of removing waypoints. During the sea trials described in Section IV this was never performed.

C. Operational Constraints and Implementation Issues

To coordinate glider fleets during AOSN II numerous issues relating to glider control and actuation, planning and information latencies, and surfacing asynchronicities were addressed.

Two critical glider control and actuation issues were constant speeds and external currents. In AOSN II, the Slocum gliders were programmed to servo to a constant pitch angle (down for diving and up for rising). This configuration yields speeds relative to external currents that are fairly uniform on time scales that span multiple yos. In this respect, the Slocum glider is suitably modeled as having constant speed. The constant speed constraint restricts what formations are feasible using VBAP. Formations that are not kinematically consistent with the speed constraint will not converge properly. For example, a "rolling" formation defined by a virtual body that is simultaneously translating and rotating is not kinematically consistent with the constant speed constraint. This is because each vehicle must slow down at some point to be "overtaken" by its neighbor. Convergence problems may also arise for certain initial conditions. For a further discussion of implementation and consequences of the constraint, see [16] and [17].

When external currents that vary across the formation are present, the very existence of a formation, i.e., a configuration of vehicles in which all relative velocities between vehicles remains zero, is uncertain. This is an artifact of the assumption that the glider speed is constant relative to the current. We circumvent this problem by using a group average current estimate in the VBAP planner [16], [17]. A related challenge can arise from using the previous glider current estimate from the previous dive cycle for the next dive cycle. Because of this, the glider may find it difficult to navigate through currents that vary greatly over short spatial scales.

As mentioned in Section III-B, we do not impose synchronous surfacings of the glider fleet. Variabilities across the glider fleet such as w-component (vertical) currents and the local bathymetry increase the likelihood of asynchronous surfacings. Also, substantial winds and surface traffic (like fishing boats, etc.) render waiting on the surface to impose synchronicity impractical and dangerous. As discussed, we generate a plan using VBAP for the entire fleet simultaneously, starting at the expected surfacing of the lead glider. For gliders yet to surface, it is tempting to consider not using the plans generated then, but instead to generate new plans based on the latest data from the lead or other glider if available. However, during the replanning process, we would have to constrain the trajectories of gliders that have already received their plans and have gone underway. VBAP is not capable of handling such a constraint. Underwater acoustic communication, if implemented, could alleviate this constraint by permitting a replan for vehicles that are already underwater. In this case, there would likely be constraints on the separation distance between gliders to enable effective communication.

Latency was also a significant issue for coordinating glider fleets. During AOSN II, data sent to the GDS after a glider surfaced was not available in a timely enough manner to be used in the generation of the next mission plan. Therefore, GPS fixes and local current estimates were latent by one dive cycle. There are two related issues which arise from this latency. First, the external current estimates lag the cycle for which we are planning by two dive cycles. That is, we are using the average current from the previous cycle as a proxy for the current during the cycle after next. Second, the currents used to estimate each glider's diving position lags by one cycle.

D. Adaptive Sampling

A central objective in ocean sampling experiments with limited resources is to collect the data that best reveals the ocean processes and dynamics of interest. There are a number of metrics that can be used to define what is meant by the best data set, and the appropriate choice of metric will typically depend on the spatial and temporal scales of interest. For example, for a broad area, the goal might be to collect data that minimizes estimation error of the process of interest. For smaller scales, the goal may be to collect data in and around features of interest, e.g., to sample at locations of greatest dynamic variability. A fundamental problem is to choose the paths of available mobile sensor platforms, notably sensor-equipped AUVs, in an optimal way. These paths do not need to be predetermined, but instead can be adapted in response to sensor measurements directly and/or output of data assimilating ocean models. This is what we refer to as adaptive sampling.

When multiple AUVs are available, cooperative feedback control is an important aspect of adaptive sampling. For example, in covering a broad region, the AUVs should be controlled to appropriately explore the region and avoid approaching one another (in which case they run the risk of becoming redundant sensors). This strategy for cooperative control and adaptive sampling with multiple AUVs is developed in [24]. For adaptive feature tracking, the formation control, gradient climbing, and front tracking described in Section II can be used. Feedback plays several critical roles. First, feedback can be used to redesign paths in response to new sensor measurements. Of equal importance, feedback is needed to manage the uncertainty inherent in the dynamics of the vehicles in the water. Using the measurements of vehicle positions and local currents, feedback (e.g., as described in Section III-C) can be used to increase robustness to disturbances.

Adaptive sampling strategies using formations are explored and implemented (using VBAP) in [16] and [17]. In [17], a library of basic formation maneuvers, such as gradient climbing, zigzagging in formation, group expansions, and rotations, are used as building blocks in scenarios for feature tracking and sampling of dynamic regions of interest.

IV. Sea Trials: AOSN II, Monterey Bay, 2003

During the AOSN II experiment in Monterey Bay in the summer of 2003, we had the opportunity to demonstrate our coordinated control methodology on Slocum glider fleets. In this section, we describe three demonstrations and present an evaluation of the coordination performance. During all three demonstrations, each glider surfaced every 2 h for a GPS fix and an updated mission plan. The gliders dove to a maximum depth of 100 m.

The first two sea trials performed on August 6, 2003 and August 16, 2003 demonstrate our ability to coordinate a group of three Slocum underwater gliders into triangle formations. In both cases, we used our VBAP methodology with a single virtual leader serving as the virtual body. We explored various orientation schemes and intervehicle spacing sequences as the formation made its way through the bay. During the last demonstration, performed on August 23, 2003, a single Slocum glider was controlled to track the path of a Lagrangian drifter in real-time. Waypoints were designed according to an algorithm that required estimates of the future drifter location so that the glider would zigzag back and forth across the path of the drifter. VBAP was not needed since there was only a single glider. However, the concept applied to a group of gliders would make use of VBAP with the path of the virtual body centroid directed to follow the desired zigzag path.

The glider dead reckoning and current estimate histories are postprocessed to estimate each glider's trajectory during the course of each demonstration. Glider position data in latitude and longitude is converted to local (Euclidean) coordinates using the *universal transverse mercator* (UTM) projection. Denote the ith glider's position at time t in the horizontal plane as $g_i(t)$. (Note: $g_i(t)$ is distinguished from $x_i(t)$ which refers to the position of the ith glider at time t as planned by VBAP.) The instantaneous formation center of mass is defined as $\bar{g}(t) = (1/N)\sum_{i=1}^{N} g_i(t)$ where N is the number of vehicles in the formation. The intervehicle distance between gliders is given by $d_{ij}(t) = \|g_i(t) - g_j(t)\|$ where $i, j = 1, \ldots, N, i \neq j$.

With a single virtual leader, the virtual body is a point and, therefore, has no orientation. In portions of the Monterey Bay sea trials, we let the orientation of the formation remain unconstrained. In principle, this means that the formation can take any orientation around the virtual leader as it moves with the virtual leader. In the case of significant currents and limited control authority, this approach allows us to dedicate all the control authority to maintaining the desired shape and size of the formation. Sometimes, however, it is of interest to devote some control authority to control the orientation. For instance, to maximize the trackline separation for improved sampling, we ran portions of the sea trials with one edge of the formation triangle perpendicular to the formation path. To effect this, we defined the desired orientation of the formation by constraining the direction of the relative position vectors $(x_i - r)$ (the vector from virtual leader to ith vehicle). Potential functions V_r as described in Section II were used to impose this constraint.

Let $r(t)$ be the VBAP planned (continuous) trajectory for the virtual leader. Since the virtual body consists only of one virtual leader, this trajectory is *the trajectory of the desired center of mass (centroid) of the formation*. A new mission is planned every 2 h and defines a 2-h segment of the demonstration; the start of each mission is defined by the time at which the lead glider dives after having surfaced. Thus, for a demonstration lasting $2K$ h, VBAP generates K missions. The *formation centroid error* at time t is defined as $\epsilon = \|\bar{g}(t) - r(t)\|$, i.e., it is the magnitude of the error between the formation centroid and the virtual leader position generated by VBAP at time t. We note that this error defines a rather conservative performance metric because it requires, for good performance, that the formation track the virtual body both in space and in time.

A. August 6, 2003: Glider Formation at Upwelling Event

On August 6, 2003, three Slocum gliders were coordinated into a triangle formation and directed towards the northwest part of Monterey Bay in response to the anticipated onset of an upwelling event (see Fig. 5). The WHOI gliders, numbered WE07, WE12, and WE13, were initially holding station at the mouth of the bay and the overall objective was to transit the gliders

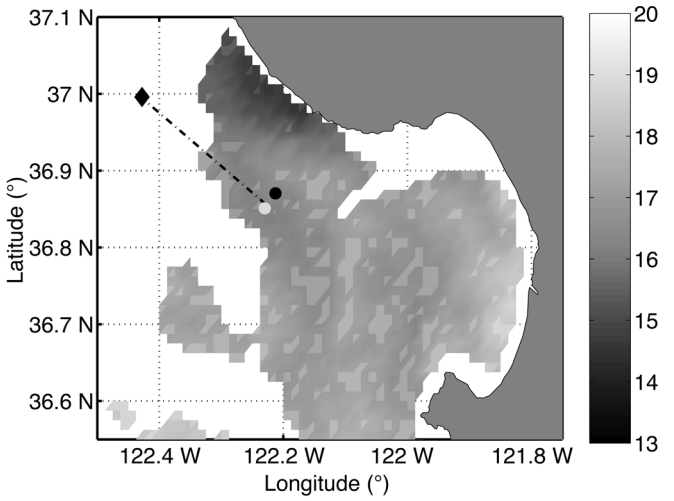

Fig. 5. Satellite sea-surface temperature (degrees Celsius) in Monterey Bay for August 6, 2003, 19:02:00Z. Cold water region near the northwest entrance of the bay indicates possible onset of upwelling event. The three solid circles indicate the starting locations of the Slocum gliders at approximately 18:00:00Z. The solid diamond is the desired destination of the glider group. Advanced very high-resolution radiometer/high-resolution picture transmission (AVHRR/HRPT) data provided courtesy of National Oceanic and Atmospheric Administration (NOAA) National Weather Service (NWS) Monterey office and NOAA National Environmental Satellite Data and Information Services (NESDIS) CoastWatch program.

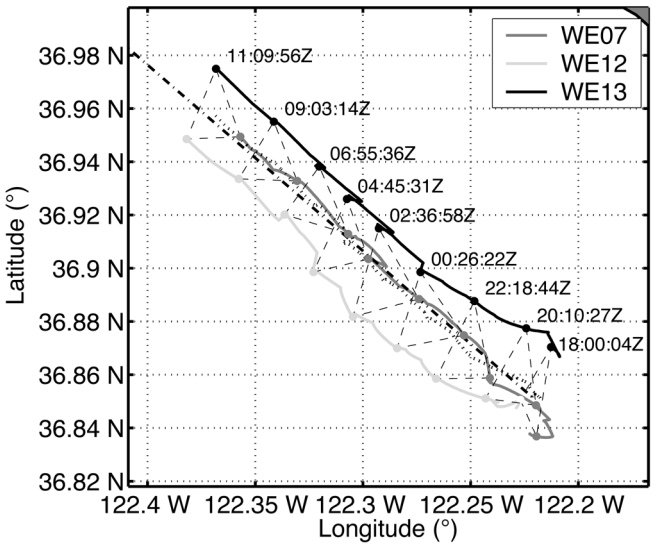

Fig. 6. Glider trajectories and snapshots of glider formations for August 6, 2003 demo. Solid lines are glider trajectories. Black dashed lines illustrate instantaneous formations at 2-h intervals. Dotted line is formation centroid. Black dash–dot line is virtual leader's trajectory (desired trajectory of formation centroid). Experiment begins at 18:00:00Z August 06, 2003.

to the northwest in an equilateral triangle formation with an intervehicle spacing of 3 km. The entire demonstration spanned 16 h, i.e., eight 2-h missions. During the first four missions, the triangle formation was free to rotate about the virtual leader. During the last four missions, the orientation of the group about the virtual leader was controlled so that an edge of the triangle formation would be perpendicular to the group's path.

Fig. 6 presents the glider trajectories and instantaneous glider formations. Starting from their initial distribution, the gliders

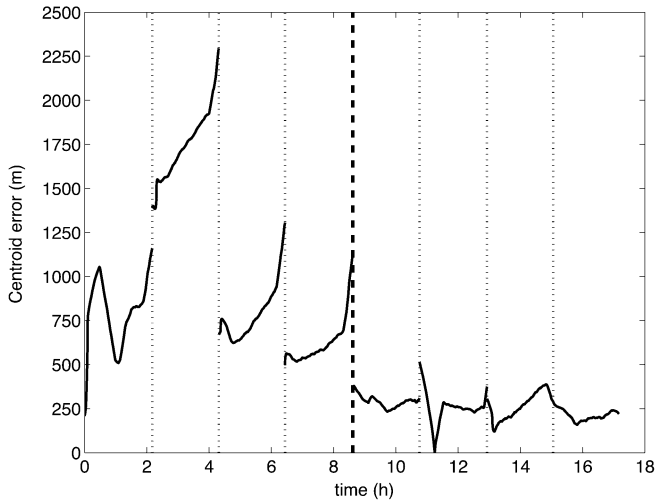

Fig. 7. Formation centroid error ϵ versus time for August 6, 2003 demo. Black dotted vertical lines indicate the beginning of each mission. Heavier black dashed vertical line indicates when orientation control was activated (time = 8.6 h).

expanded to the desired configuration while the formation centroid tracked the desired reference trajectory, i.e., the virtual leader. As shown, the group did maintain formation while transiting. At 02:36:00Z, orientation control was activated and by 06:55:00Z the group had noticeably reoriented itself. As a result of generating waypoint plans that respect a glider with constant speed, some degree of reverse motion is seen to occur during the initial creation of the desired formation and during the missions when orientation control was active.

The formation centroid error ϵ is plotted over all eight missions in Fig. 7 as a function of time t. The mean value of ϵ averaged over all eight missions is 623 m with a standard deviation of 500 m. The average error over the last four missions is 255 m with a standard deviation of 67 m. The discontinuity at each mission replan is a result of reinitializing the virtual leader at the expected centroid of the group. The error across the discontinuity gives insight into how well we predicted the initial location of the group centroid at the start of each mission. During mission two, the algorithms performed worst at predicting initial centroid location and maintaining the distance between the actual and desired centroid location. This error corresponds to the largest error between the current estimates fedforward into the glider simulator and VBAP (see Fig. 4), and the estimated current measured by the gliders at the end of that mission. The algorithms performed best with respect to this metric during the last four missions. It is possible that the difference in performance is related to our observations that during the latter part of the demonstration each glider travelled fastest relative to ground due to more favorable currents in the glider's direction of travel.

Fig. 8 portrays the magnitude of the error in intervehicle distance $d_{ij}(t)$ versus time for the three glider pairings WE07–WE12, WE07–WE13, and WE12–WE13. The mean error of all three pairings is 423 m, roughly 14% of the desired spacing of 3 km, with a standard deviation of 159 m. The mean intervehicle spacing error was largest during missions two and five.

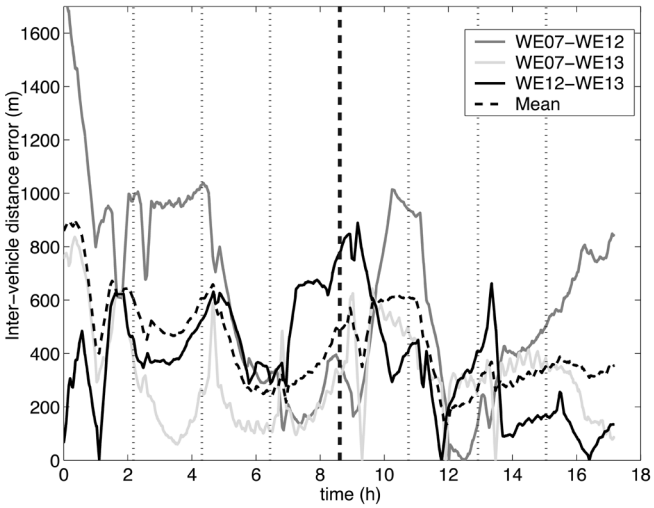

Fig. 8. Magnitude of interglider distance error versus time for August 6, 2003 demo. Black dotted vertical lines indicate the beginning of each mission. Heavier black dashed vertical line indicates when orientation control was activated (time = 8.6 h).

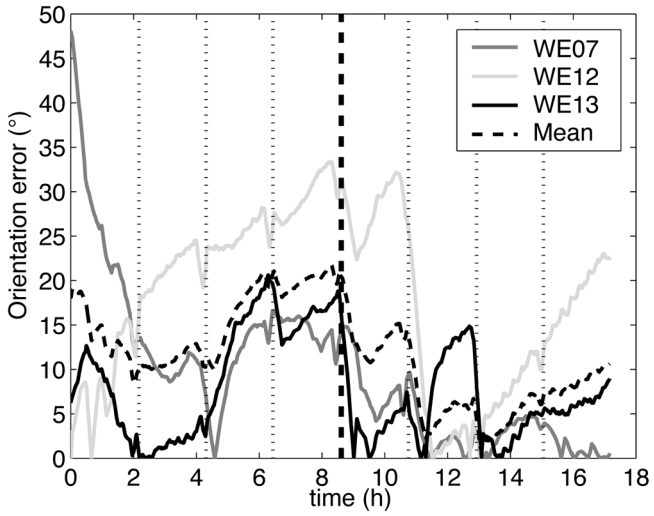

Fig. 9. Magnitude of orientation error versus time for August 6, 2003 demo. Black dotted vertical lines indicate the beginning of each mission. Heavier black dashed vertical line indicates when orientation control was activated (time = 8.6 h).

Formation orientation error versus time is portrayed in Fig. 9. The desired orientation was chosen to have an edge of the formation perpendicular to the line from the initial virtual leader location at the start of each mission to the final destination, with two vehicles in the front, side-by-side, and one vehicle trailing. The control is designed so that any of the vehicles can play any of the roles, i.e., we do not assign a particular vehicle to a particular place in the oriented triangle. As shown in Fig. 6, WE07 was the trailing glider and WE12 and WE13 the leading gliders in the triangle formation. The error for a given glider plotted in Fig. 9 is computed as the difference between the desired angle of the ideal glider position relative to the virtual leader position (θ_{ik} in Fig. 1) and the angle of the measured glider position relative to the formation centroid.

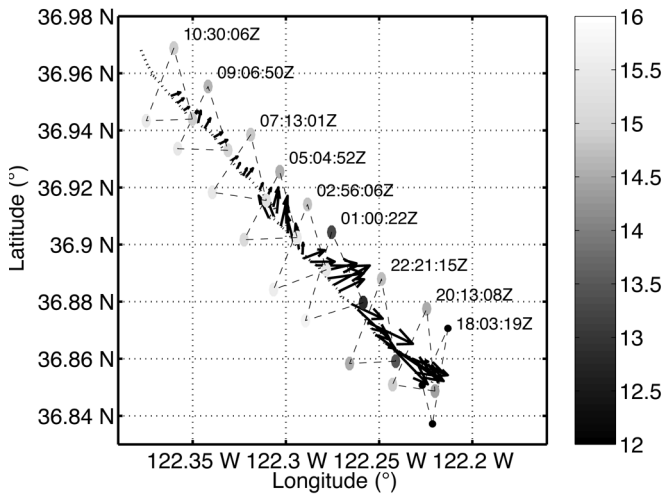

Fig. 10. Glider formation and minus the least-square temperature gradient estimates at the instantaneous formation centroid for August 6, 2003 demo. Each dot represents a glider location and is shaded to indicate its temperature measurement in degrees Celsius. Experiment begins at 18:00:00Z August 06, 2003.

For comparison purposes, we plot the error during the first four missions, when the orientation of the group was not controlled, and during the last four missions when the orientation was controlled. During missions three and four, the mean orientation error was 18.2° with a standard deviation of 7.8°. We do not concern ourselves with the first two missions since the orientation is in a state of flux while the formation is expanding or contracting to achieve the desired intervehicle and vehicle-to-virtual-leader spacings. During missions five through eight, the mean orientation error was reduced to 8.1° with a standard deviation of 8.1°.

To examine the ability of the formation to serve as a sensor array and detect regions of minimum temperature, we computed least-square gradient estimates of temperature given each glider's temperature measurements. The negative of these least-square gradient estimates, $-\nabla T_{\rm est}$ (to point to cold regions), are shown as vectors in Fig. 10. These gradients are computed using data measured at 10-m depth for comparison with the available AVHRR satellite–sea-surface–temperature (SST) data. All glider temperature measurements and their respective locations which fall within a 0.5-m bin around the 10-m isobath are extracted from the postprocessed glider data. Values within each bin are then averaged. Since the gliders travel asynchronously through depth, we interpolated the data as a function of time. For simplicity, we chose to compute the gradients at the times associated with the lead (WE12) glider's binned measurements. More precise filtering can be performed by using all past measurements and associated spatial and temporal covariances to provide the best measurement estimates at a given location [16]. Comparison with Fig. 5 illustrates that the estimated negative gradient vector points correctly to the cold water near the coast at the northwest entrance of the bay.

B. August 16, 2003: Multiasset Demonstration

On August 16, 2003, a formation of three Slocum gliders was directed to travel in a region simultaneously sampled by

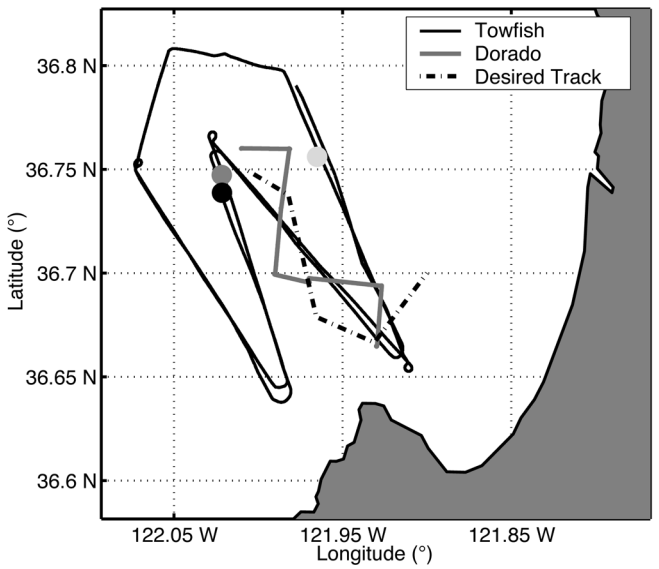

Fig. 11. August 16, 2003 demonstration. Black line is towfish trajectory. Gray line is Dorado trajectory. Shaded dots denote initial locations of gliders WE05, WE09, and WE10, respectively. Black dash–dot line is desired formation centroid trackline. The towfish begins at 15:07:00Z and finishes two transects of the "W" pattern by 03:20:00Z August 17, 2003. The Dorado vehicle begins its single transect at 14:19:00Z August 16, 2003 and finishes at 17:58:00Z. The gliders start at 14:11:00Z August 16, 2003 and finish at 06:17:00Z August 17, 2003.

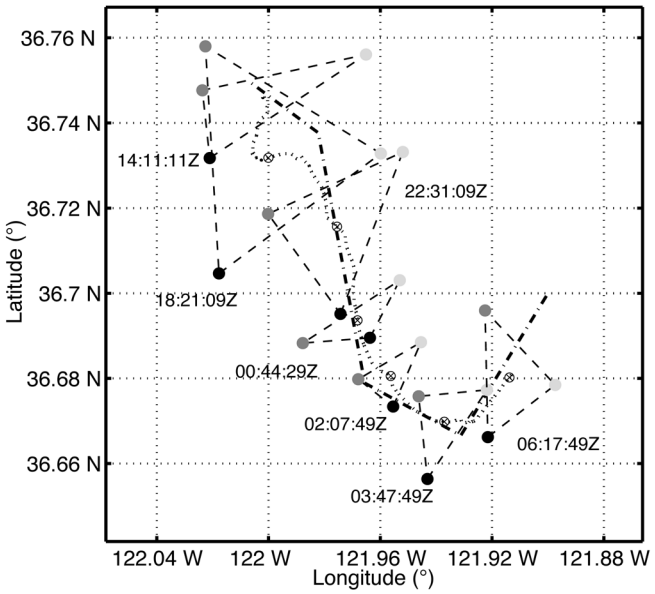

Fig. 12. Glider formation snapshots for August 16, 2003 demo. Black dashed lines illustrate instantaneous formations. Black dotted line is formation centroid. Black dash–dot line is virtual leader path, i.e., desired centroid trajectory. Experiment begins at 14:11:00Z August 16, 2003.

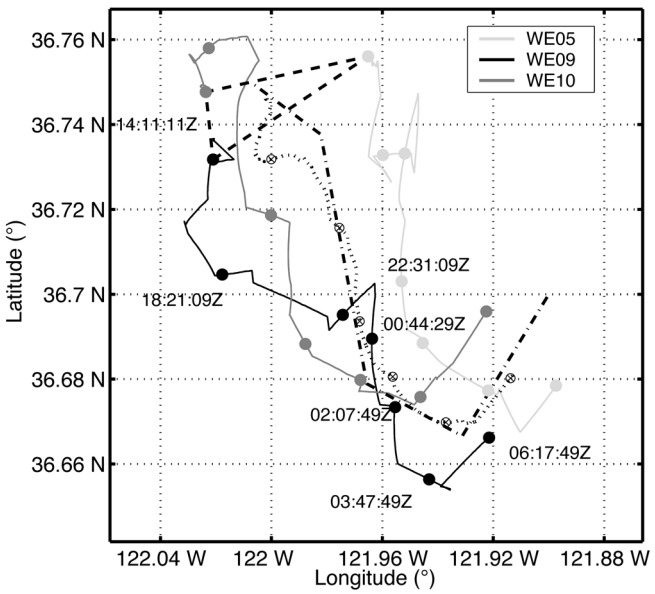

Fig. 13. Glider trajectories for August 16, 2003 demo. Solid lines are glider trajectories. Black dotted line is formation centroid. Black dash–dot line is virtual leader path, i.e., desired centroid trajectory. Experiment begins at 14:11:00Z August 16, 2003.

a ship dragging a towfish sensor array and the MBARI propeller-driven AUV Dorado. The towfish and Dorado measurements provide an independent data set by which to corroborate the glider formation's sampling abilities.

As discussed in Section I, the mobile observation platforms should be used so that their capabilities are compatible with the spatial and temporal scales of interest. The towfish, Dorado, and gliders can be used to resolve different length and time scales. For example, the towfish is much faster than the Dorado and the gliders, whereas the Dorado is up to three times faster than the gliders. Some analysis of sampling capabilities based on a metric computed from estimation error of the sampled process of interest is presented at the end of this section.

Fig. 11 illustrates the towfish and Dorado trajectories, the initial positions of the three gliders and the desired trackline of the glider formation centroid. The WHOI gliders WE05, WE09, and WE10 were initially holding station near the center of the bay, and the overall objective was to crisscross a region to the southeast while in an equilateral triangle formation. The entire trial spanned seven 2-h missions. The desired intervehicle distance was set to 6 km for the first three missions and reduced to 3 km thereafter. The orientation of the desired triangle formation was controlled with one triangle edge normal to the virtual body path throughout the entire demonstration. The virtual leader followed the piecewise linear path shown as the black dash–dot line in Fig. 11.

Fig. 12 presents the instantaneous glider formations and Fig. 13 presents the glider trajectories during the demonstration. Starting from their initial distribution, the gliders expand to the desired spacing and orientation while the group centroid attempts to track the desired reference trajectory. In Fig. 12, we see that the group centroid had a difficult time staying near the reference trajectory in space for the first few missions.

The formation centroid error ϵ is plotted in Fig. 14 as a function of time t. The mean value of ϵ averaged over all seven missions is 732 m with a standard deviation of 426 m. The worst performance is seen to occur during mission five. As on August 6, 2003, this error corresponds to the largest error between the current estimates fedforward into the glider simulator and VBAP, and those estimated by the gliders at the end of that mission. In general, the methodology did not perform as well with

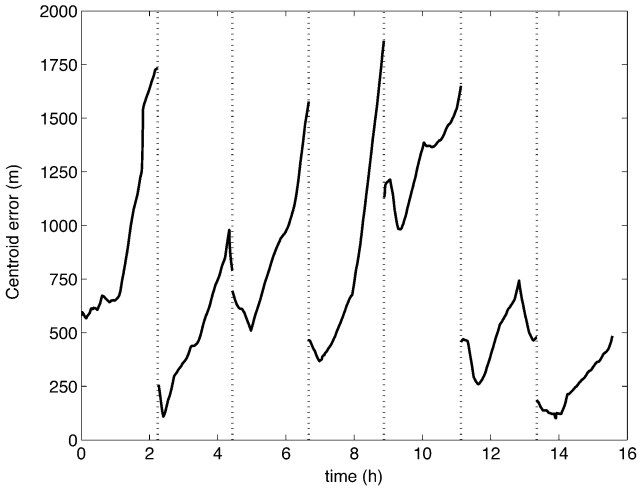

Fig. 14. Formation centroid error ϵ versus time for August 16, 2003 demo. Black dotted vertical lines indicate the beginning of each mission.

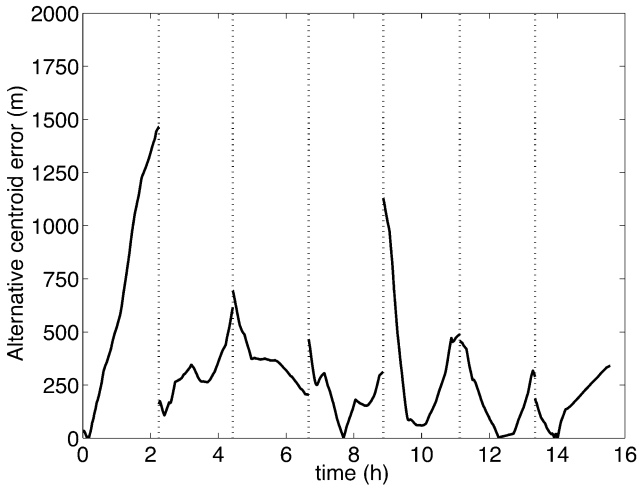

Fig. 15. Alternate formation centroid error ε' versus time for August 16, 2003 demo. Black dotted vertical lines indicate the beginning of each mission.

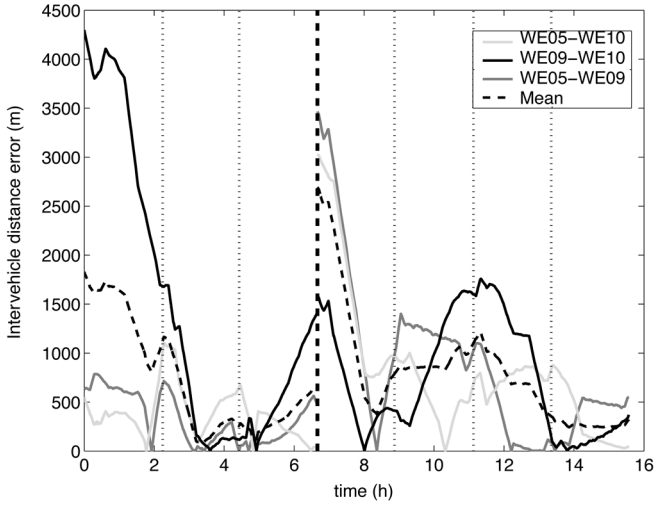

Fig. 16. Magnitude of interglider distance error versus time for August 16, 2003 demo. Black dotted vertical lines indicate the beginning of each mission. Heavier black dashed vertical line indicates when desired intervehicle spacing was decreased from 6 to 3 km (time = 6.7 h).

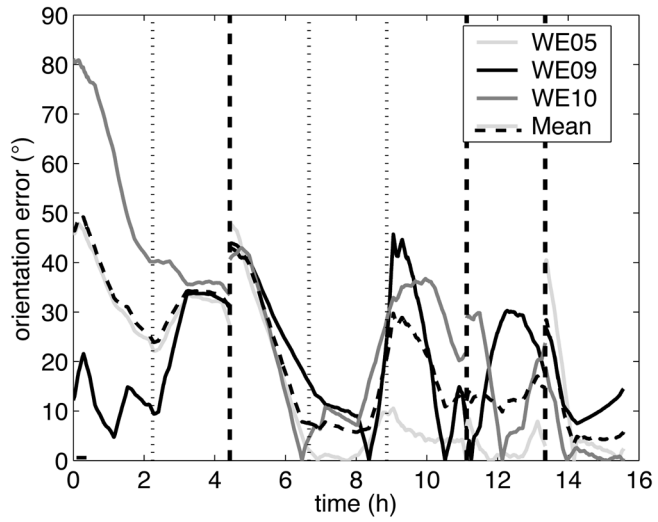

Fig. 17. Magnitude of orientation error versus time for August 16, 2003 demo. Black dotted vertical lines indicate the beginning of each mission. Heavier black dashed vertical line indicates when desired orientation changed to reflect change in virtual body direction (time = 4.4, 11.2, and 13.4 h).

respect to this metric as it did on August 6, 2003. One difference of note is the significantly stronger currents experienced on August 16, 2003, exceeding 30 cm/s on more than one occasion (cf. the glider estimated speed relative to water is 40 cm/s).

A less conservative metric can be defined by

$$\varepsilon'(t) = \min_{w \in \Gamma} \|\bar{g}(t) - w\|$$

where Γ is the set of all points along the path of the virtual leader. This measures centroid tracking performance in space without regard to time. Fig. 15 presents ε' for this demonstration as a function of time t. By this metric, the methodology performs quite well for the latter part of the experiment which is consistent with Figs. 12 and 13. In particular, the mean error overall is 471 m with a standard deviation of 460 m. For missions four through seven, the mean error is 210 m with a standard deviation of 118 m.

The magnitude of the intervehicle distance error versus time for the three glider pairings WE05–WE09, WE05–WE10, and WE09–WE10 is presented in Fig. 16. For missions two and three, the mean error over all three pairings was 394 m, roughly 7% of the desired spacing of 6 km, with a standard deviation of 270 m. For missions five through seven, the mean error over all three pairings was 651 m, roughly 22% of the desired 3-km spacing, with a standard deviation of 312 m. During this period, the average intervehicle distance was less than the desired 3 km.

The orientation error is plotted in Fig. 17. The discontinuities reflect changes in the desired orientation of the reference formation which were allowed to occur only at the beginning of a mission. The mean orientation error for mission two was 31° with a standard deviation of 3°. This corresponds to the period when the formation centroid was having difficulty staying on the desired trackline. At mission three, the first change in desired reference formation orientation occurred. The mean orientation

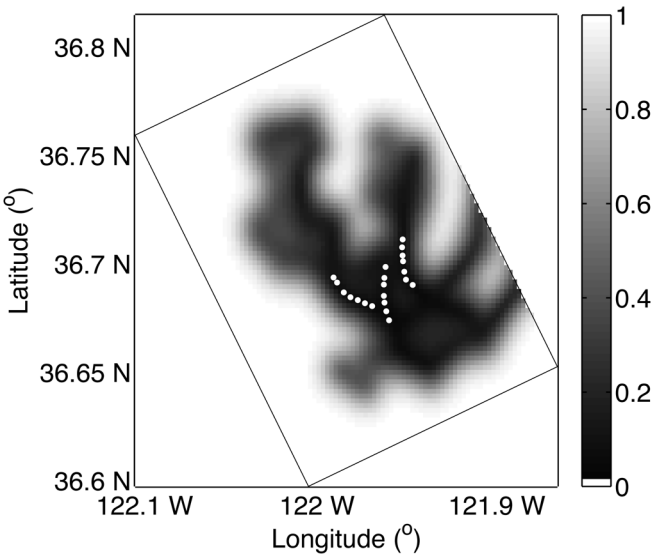

Fig. 18. OA error map for gliders with $\sigma = 1.5$ km and $\tau = 1$ d for August 16, 2003 demo.

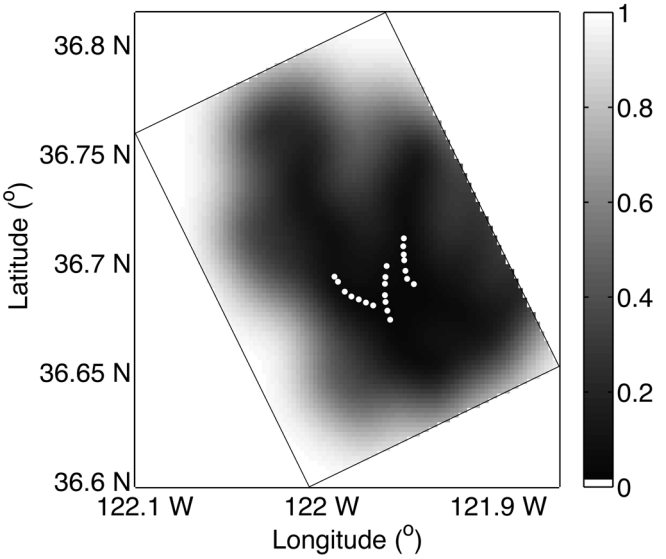

Fig. 19. OA error map for gliders with $\sigma = 3.0$ km and $\tau = 1$ d for August 16, 2003 demo.

error during missions three through five, was 18° with a standard deviation of 11°. The large standard deviation reflects the relatively lower orientation error during missions three and four as compared with mission five. The next desired reference formation orientation change occurred at mission six and the final change occurred at mission seven. For mission six, the mean orientation error was 13° with a standard deviation of 2°. For mission seven, the mean orientation error was 9° with standard deviation of 7°. Both the mean intervehicle distance error and the mean orientation errorexhibit similar trends during missions five and six. Recall that the formation centroid error was also largest during mission five which corresponds to the largest variation between fedforward currents and those actually experienced.

1) Objective Analysis of August 16, 2003 Demonstration: To quantitatively assess sampling performance, we computed the objective analysis (OA) error map for the August 16, 2003 demonstration. OA is a simple data assimilation scheme that provides a means to compute a useful metric for judging performance of a sampling strategy [13], [25]–[27]. We discuss application of this method to adaptive ocean sampling in [24]. A performance metric for evaluating sensor arrays is the square root of the variance of the error of the OA estimator. Using this metric, a gridded error map can be computed using the location of measurements taken, the assumed measurement error, and the space–time covariance of the process of interest. In what follows, we assume a spatially homogeneous and isotropic process. We use an autocorrelation function which is Gaussian in space and time with spatial scale σ, and temporal scale τ, following [28]. The scales σ and τ are determined by *a priori* statistical estimates of the process. Specifically, σ is the $1/e$ spatial decorrelation scale, τ is the $1/e$ temporal decorrelation scale, and we take 2σ to be the zero-crossing scale. In the absence of *a priori* statistics, these parameters can be chosen to evaluate the sampling performance of signals at the specified scales.

We have computed gridded error maps for August 16, 2003 at 00:00:00Z with $\tau = 1$ d, $\sigma = 1.5$ km and $\sigma = 3.0$ km,

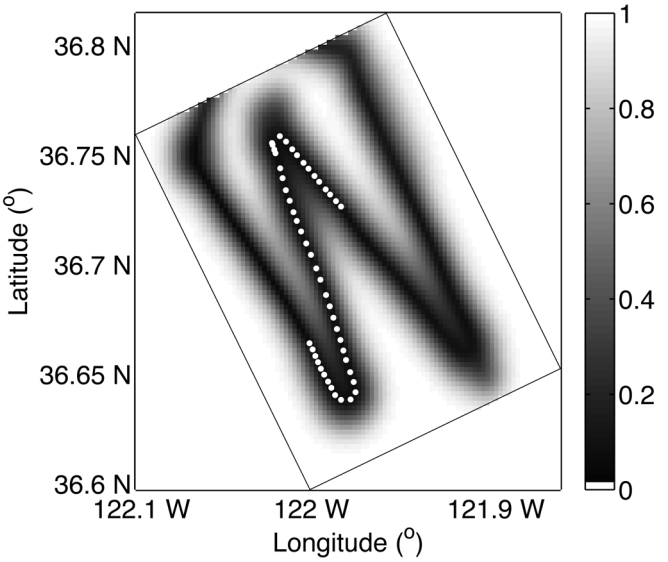

Fig. 20. OA error map for towfish with $\sigma = 1.5$ km and $\tau = 1$ d for August 16, 2003 demo.

and measurement error variance 10% of the (unit) process variance. The map dimensions are 14 km $\times$ 20 km. The maps use measurements over a 4-h window centered on the time of the map (00:00:00Z). The measurement locations for the 2-h span starting with the map time are plotted as white dots. For the gliders, each measurement corresponds to data collected during one yo of a glider. The maps for the gliders are shown in Figs. 18 and 19. The error map for the towfish with $\sigma = 1.5$ km is shown in Fig. 20. The measurement locations for the towfish are the locations of the 25-m depth crossings.

Note that σ determines the cross-track width of the sensor swath. At 3-km spacing of the glider formation, the root-mean-square (rms) estimate error at the center of the glider formation is 0.2 for $\sigma = 3$ km and 0.05 for $\sigma = 1.5$ km. According to this metric, the triangle formation with 3-km spacing gives very good error reduction at its centroid when the spatial scale is

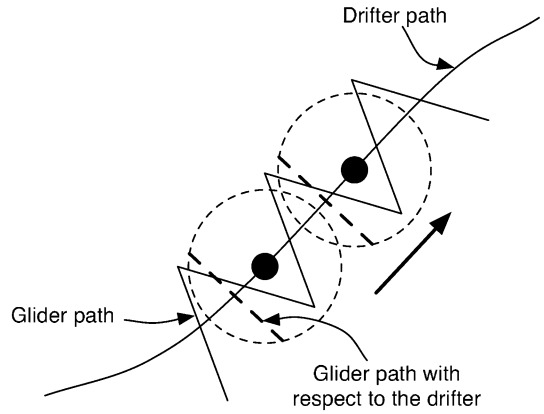

Fig. 21. Drifter tracking plan schematic: The solid circles indicate drifter positions at two time instants, and the line connecting the solid circles is the drifter path. The solid line crossing the drifter path is the desired glider path. The glider path with respect to the drifter is a chord of a circle of specified radius about the drifter.

defined by $\sigma = 3$ km (and the temporal scale by $\tau = 1$ d) and excellent accuracy in estimation of the process along the path of its centroid when $\sigma = 1.5$ km.

Following [24], we consider the role of the dimensionless *sampling number*, $S\mathfrak{p} = (v\tau/\sigma)$, where v is the vehicle speed. In this example, $S\mathfrak{p}$ determines the along-track length of the sensor swath. The effective $S\mathfrak{p}$ is about 10 for the gliders, 30 for the Dorado, and 300 for the towfish at $\sigma = 3$ km and $\tau = 1$ d. For these values of σ and $S\mathfrak{p}$, the glider formation orientation accuracy is more important than intervehicle spacing accuracy. Orientation accuracy (to ensure maximum trackline separation) will enlarge the array sampling footprint by reducing overlapping sensor swaths.

C. August 23, 2003: Drifter Tracking

In this sea trial, we controlled a Slocum glider to follow a Lagrangian drifter in real time. This sea trial was meant to demonstrate the utility of the glider to track Lagrangian particle features such as a water mass encompassing an algae bloom.

During the experiment, the drifter transmitted its position data approximately every 30 min. The data arrived at the command station with a 15-min lag. To follow the drifter in real time, it was necessary to predict the future trajectory of the drifter. This prediction was based on a persistence rule, using a quadratic or a linear curve fit of measured positions and corresponding time stamps.

The persistence rule was used to estimate the following:

1) the position of the drifter at the next estimated surfacing time of the glider;
2) the average speed of the drifter during the following glider dive cycle.

The previous information was used in conjunction with the estimated surfacing location of the glider (calculated using the glider simulator described in Section III-B) to determine the glider waypoint list. The glider surfaced approximately every 2 h as in the demonstrations described previously.

The goal of this demonstration was to have the glider travel back and forth along a chord of a circle in a reference frame attached to the drifter, as shown in Fig. 21. The center of the circle was at the drifter location. The radius of the circle and the distance of the chord from the center of the circle were specified. Fig. 22 shows the actual tracks followed by the drifter and the glider during the demonstration. On the left panel, the glider path can be seen to follow approximately the shape of the drifter path. The closeup on the right panel reveals how effectively the glider crisscrossed the drifter path. In Fig. 22, we see that starting from the dive cycle beginning at X, the glider travelled along straight sections, followed by a zigzag motion, and then a change in the direction of motion. The straight sections correspond to the glider catching up with the drifter at the start of a new dive cycle. Once the glider dead-reckoned position is close to the drifter position estimated by the glider, the glider starts the zigzag swaths in an attempt to move along a chord of a circle with respect to the drifter.

The estimated currents onboard the glider and the currents experienced by the drifter were significantly different. The drifter motion was governed by near-surface currents due to the "holey-sock" drifter design [29], whereas the glider motion was subjected to the integrated effect of currents throughout its profiling depth. The difference in the currents affecting the two platforms contributed to the difficulty in the glider tracking the drifter. Moreover, the drifter trajectory during the time the glider was in the water had to be estimated using a persistence rule as described earlier. Since the glider surfaced only every 2 h, it was given waypoints that were based on a 2-h estimation of drifter trajectory. This estimation was generally not accurate with the drifter trajectory persisting less than 2 h.

The average speed of the drifter during this demonstration was approximately 7 cm/s. Towards the end of the experiment the drifter moved much slower and its displacement in half an hour was less than the GPS resolution. As a result, the drifter appeared stationary on the GPS scale. The glider caught up with the drifter quickly, but unknown speed fields, time delays in the control implementation, and the limited sensitivity of the GPS contributed to errors in tracking. Additionally, a bug in the waypoint calculation code also introduced errors in the first few dive cycles of the experiment.

To improve the accuracy of drifter tracking, one could modify this approach slightly to follow the actual path traced by the drifter with a slight delay, instead of tracking an estimated trajectory in real time. This way the glider would be able to cross the drifter path several times. The frequency and amplitude of cross-path swaths of the glider could be adjusted based on the drifter speed. This strategy induces a tracking time delay at least on the order of the glider surfacing period, which was 2 h in our demonstration. Such a time delay may be acceptable, especially since the tracking accuracy may be greatly improved. For small drifter speeds, the glider could be asked to "hold station" at the last drifter position.

V. Final Remarks

We have described a method for cooperative control of multiple vehicles that enables adaptable formation control and missions such as gradient climbing in a sampled environment. This method has been implemented on a fleet of autonomous underwater gliders which have high endurance but move slowly and are sensitive to currents. Results are described from several sea

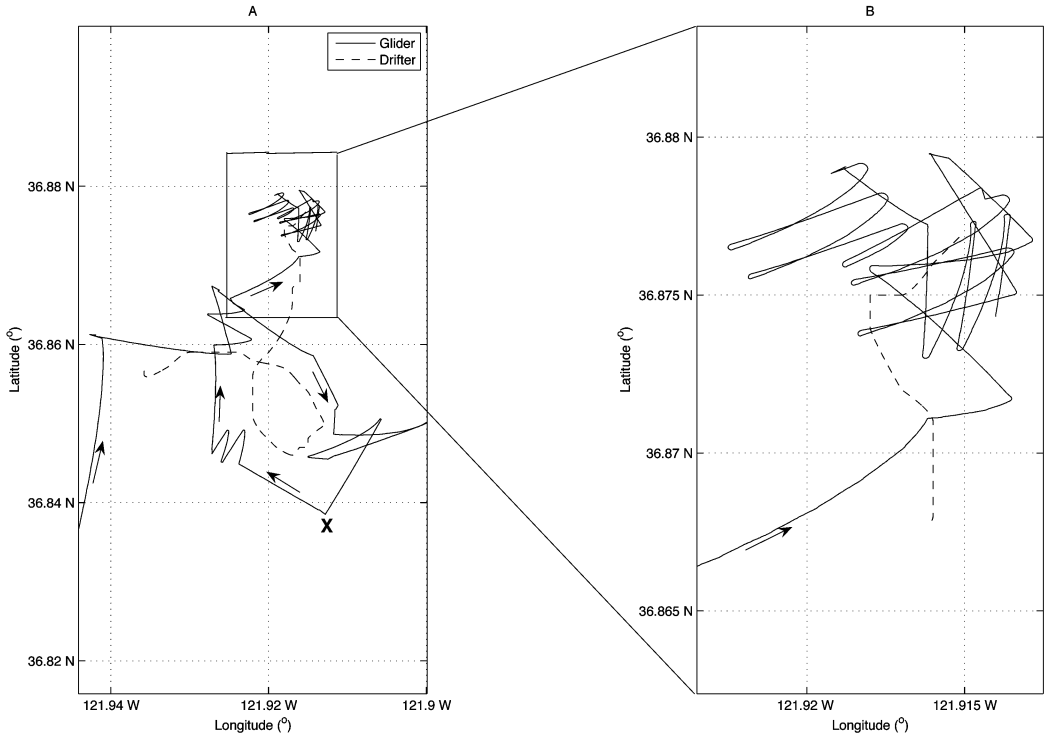

Fig. 22. Tracks followed by the glider and the drifter during the August 23, 2003 demo. (A) Complete demonstration. (B) Last four glider dive cycles—the dashed line is the drifter track and the solid line is the glider track.

trials performed in August 2003 in Monterey Bay. These results show that groups of AUVs, namely gliders, can be controlled as formations that move around as required, maintaining prescribed formation orientation, and intervehicle spacing with reasonably good accuracy for the application despite periods of strong currents and numerous operational constraints. An approach under development to further improve performance in the presence of currents involves using a model of the tides.

Temperature gradient estimates computed from onboard glider temperature measurements taken during these sea trials are shown to be smooth and at least qualitatively well correlated with temperature fields measured by satellite. These results suggest good potential for cooperative formation control in gradient climbing and feature tracking for physical and biological processes.

Feature tracking can contribute to adaptive ocean sampling strategies, especially for estimating processes at smaller scales. As part of the analysis of the August 16, 2003 demonstration, we examined the capability of the glider groups and other mobile sensor platforms to sample for the purpose of minimizing estimation error of a process of interest given *a priori* statistics for the process. A metric based on this objective analysis error can be used to judge sampling performance for a sensor array. This metric, which looks at minimization of estimation error, is directly related to maximization of entropic information.

This metric can also be used to derive optimal sensor array designs. In ongoing work, we examine optimal sensor array designs for vehicle groups in broad-area coverage problems using this and related metrics. We also develop alternative cooperative control strategies well suited to the broad-area coverage problem (see, for example, [24]). Sea trials are planned for 2006 as part of the ASAP project [5].

ACKNOWLEDGMENT

The authors would like to thank all of the other AOSN team members for support, collaboration, and easy access to relevant data. They would like to especially thank S. Haddock and J. Ryan for their help with the Dorado and the towfish in the cooperative, multivehicle demonstration on August 16, 2003 and F. Chavez for his help with the drifter for the demonstration on August 23, 2003.

REFERENCES

[1] T. B. Curtin, J. G. Bellingham, J. Catipovic, and D. Webb, "Autonomous oceanographic sampling networks," *Oceanography*, vol. 6, pp. 86–94, 1989.

[2] V. Kumar, N. E. Leonard, and A. S. Morse, Eds., *Cooperative Control: A Post-Workshop Volume, 2003 Block Island Workshop on Cooperative Control*. New York: Springer-Verlag, 2005.

[3] B. Schultz, B. Hobson, M. Kemp, and J. Meyer, "Field results of multi-UUV missions using RANGER MicroUUVs," in *Proc. MTS/IEEE Conf. OCEANS*, Sep. 2003, pp. 956–961.

[4] Monterey Bay Aquarium Research Institute (MBARI), "Autonomous Ocean Sampling Network II (AOSN II)" Collaborative Project, 2003 [Online]. Available: http://www.mbari.org/aosn/

[5] Multidisciplinary University Research Initiative (MURI) , "Adaptive Sampling and Prediction (ASAP) Collaborative MURI Project [Online]. Available: http://www.princeton.edu/~dcsl/asap

[6] O. Khatib, "Real time obstacle avoidance for manipulators and mobile robots," *Int. J. Robot. Res.*, vol. 5, pp. 90–99, 1986.

[7] P. Khosla and R. Volpe, "Superquadric artificial potentials for obstacle avoidance," in *Proc. IEEE Int. Conf. Robot. Autom.*, Apr. 1988, pp. 1778–1784.

[8] E. Rimon and D. E. Koditschek, "Exact robot navigation using artificial potential functions," *IEEE Trans. Robot. Autom.*, vol. 8, no. 5, pp. 501–518, Oct. 1992.

[9] J. H. Reif and H. Wang, "Social potential fields: A distributed behavioral control for autonomous robots," *Robot. Autonom. Syst.*, vol. 27, pp. 171–194, 1999.

[10] W. S. Newman and N. Hogan, "High speed robot control and obstacle avoidance using dynamic potential functions," in *Proc. IEEE Int. Conf. Robot. Autom.*, 1987, pp. 14–24.

[11] J. Barraquand, B. Langlois, and J. C. Latombe, "Robot motion planning with many degrees of freedom and dynamic constraint," in *Proc. 5th Int. Symp. Robot. Res.*, Aug. 1989, pp. 74–83.
[12] D. Yoerger, A. Bradley, H. Singh, and R. Bachmayer, "Surveying a subsea lava flow using the autonomous benthic explorer (ABE)," *Int. J. Syst. Sci.*, vol. 29, pp. 1031–1044, 1998.
[13] F. P. Bretherton, R. E. Davis, and C. B. Fandry, "A technique for objective analysis and design of oceanographic experiments applied to MODE-73," *Deep-Sea Res.*, vol. 23, pp. 559–582, 1976.
[14] P. Ögren, E. Fiorelli, and N. E. Leonard, "Cooperative control of mobile sensor networks: Adaptive gradient climbing in a distributed environment," *IEEE Trans. Autom. Control*, vol. 49, no. 8, pp. 1292–1302, Aug. 2004.
[15] ——, "Formations with a mission: Stable coordination of vehicle group maneuvers," in *Proc. Symp. Math. Theory Netw. Syst.*, 2002, pp. 1–15.
[16] E. Fiorelli, "Cooperative vehicle control, feature tracking, and ocean sampling," Ph.D. dissertation, Mechanical and Aerospace Engineering, Princeton University, Princeton, NJ, 2005.
[17] E. Fiorelli, P. Bhatta, N. E. Leonard, and I. Shulman, "Adaptive sampling using feedback control of an autonomous underwater glider fleet," in *Proc. Symp. Unmanned Untethered Submersible Technol.*, 2003, pp. 1–16.
[18] N. E. Leonard and E. Fiorelli, "Virtual leaders, artificial potentials and coordinated control of groups," in *Proc. 40th IEEE Conf. Decision Control*, 2001, pp. 2968–2973.
[19] F. Zhang and N. E. Leonard, "Generating contour plots using multiple sensor plots," in *Proc. IEEE Swarm Intell. Symp.*, Jun. 2005, pp. 309–314.
[20] D. L. Rudnick, R. E. Davis, C. C. Eriksen, D. M. Fratantoni, and M. J. Perry, "Underwater gliders for ocean research," *Mar. Technol. Soc. J.*, vol. 38, no. 1, pp. 48–59, 2004.
[21] D. C. Webb, P. J. Simonetti, and C. P. Jones, "SLOCUM: An underwater glider propelled by environmental energy," *IEEE J. Ocean. Eng.*, vol. 26, no. 4, pp. 447–452, Oct. 2001.
[22] J. Sherman, R. E. Davis, W. B. Owens, and J. Valdes, "The autonomous underwater glider 'Spray," *IEEE J. Ocean. Eng.*, vol. 26, no. 4, pp. 437–446, Oct. 2001.
[23] C. C. Eriksen, T. J. Osse, T. Light, R. D. Wen, T. W. Lehmann, P. L. Sabin, J. W. Ballard, and A. M. Chiodi, "Seaglider: A long range autonomous underwater vehicle for oceanographic research," *IEEE J. Ocean. Eng.*, vol. 26, no. 4, pp. 424–436, Oct. 2001.
[24] N. E. Leonard, D. Paley, F. Lekien, R. Sepulchre, D. M. Fratantoni, and R. E. Davis, "Collective motion, sensor networks and ocean sampling," *Proc. IEEE*, vol. 95, 2007, to be published.
[25] L. S. Gandin, *Objective Analysis of Meteorological Fields*. Jerusalem, Israel: Israel Program for Scientific Translations, 1965.
[26] A. Bennett, *Inverse Modeling of the Ocean and Atmosphere*. Cambridge, U.K.: Cambridge Univ. Press, 2002.
[27] E. Kalnay, *Atmospheric Modeling, Data Assimilation and Predictability*. Cambridge: Cambridge University Press, 2003.
[28] P. F. J. Lermusiaux, "Data assimilation via error subspace statistical estimation, part II: Mid-Atlantic bight shelfbreak front simulations, and ESSE validation," *Montly Weather Rev.*, vol. 127, no. 8, pp. 1408–1432, 1999.
[29] F. P. Chavez, J. T. Pennington, R. Herlien, H. Jannasch, G. Thurmond, and G. E. Friederich, "Moorings and drifters for real-time interdisciplinary oceanography," *J. Atmos. Ocean Technol.*, vol. 14, pp. 1199–1211, 1997.

Edward Fiorelli (S'04–M'05) received the B.S. degree in mechanical engineering from the Cooper Union for the Advancement of Science and Art, New York, in 1997 and the Ph.D. degree in mechanical and aerospace engineering from Princeton University, Princeton, NJ, in 2005.

From 1997-1999, he was a Mechanical Engineer at GEC Marconi Aerospace, Greenlawn, NY, where he designed radar and telecommunication equipment enclosures for military aerospace applications. In 2006, he joined the Remote Sensing and Surveillance group at Northrop Grumman, Azusa, CA. His research interests include autonomous vehicles, multiagent control design, filtering and estimation, and their applications to distributed sensor networks.

Naomi Ehrich Leonard (S'90–M'91–SM'02) received the B.S.E. degree in mechanical engineering from Princeton University, Princeton, NJ, in 1985 and the M.S. and Ph.D. degrees in electrical engineering from the University of Maryland, College Park, in 1991 and 1994, respectively.

From 1985 to 1989, she worked as an Engineer in the electric power industry for MPR Associates, Inc. Currently, she is a Professor of Mechanical and Aerospace Engineering and Associated Faculty Member of the Program in Applied and Computational Mathematics at Princeton University. Her current research interests include nonlinear control and dynamics, cooperative control, mobile sensor networks, AUVs, adaptive ocean sampling, and collective motion in animal aggregations.

Pradeep Bhatta (S'01–M'06) received the B.Tech. degree in mechanical engineering from Indian Institute of Technology Bombay, Mumbai, India, in 1998, the M.S. degree in mechanical engineering from The Pennsylvania State University, State College, in 1999, and the M.A. and Ph.D. degrees in mechanical and aerospace engineering from Princeton University, Princeton, NJ, in 2002 and 2006, respectively.

He is currently a New Jersey Technology Postdoctoral Fellow and a Senior Technical Staff at Princeton Satellite Systems, Inc., Princeton, NJ. His research interests include nonlinear analysis, estimation and control with applications to underwater and aerospace systems, multiagent control, and wind energy conversion systems.

Derek A. Paley (S'03) received the B.S. degree in applied physics from Yale University, New Haven, CT, in 1997 and the M.S. degree in mechanical and aerospace engineering from the Mechanical and Aerospace Engineering Department, Princeton University, Princeton, NJ, in 2004, where he is currently working towards the Ph.D. degree.

From 1997 to 2000, he was an Analyst in the defense industry at Metron Inc., Reston, VA. From 2000 to 2002, he was a Software Engineer in the underwater vehicle industry at Bluefin Robotics Corporation, Cambridge, MA. His research interests are in dynamics and control, specifically cooperative control, and collective motion with application to designing mobile sensor networks and modeling animal aggregations.

Ralf Bachmayer (S'98–M'03) received the engineering degree in electrical engineering from the Technische Universität Karlsruhe, Karlsruhe, Germany, in 1995 and the M.Sc. and Ph.D. degrees in mechanical engineering from The Johns Hopkins University, Baltimore, MD, in 1997 and 2000, respectively.

He is an Associate Research Officer at National Research Council of Canada's Institute for Ocean Technology and an Adjunct Professor at Memorial University, St. John's, NL, Canada. In 1995, he worked as a Visiting Researcher at the Deep Submergence Laboratory, Woods Hole Oceanographic Institution, Woods Hole, MA. From 2000 to 2003, he joined the Dynamical Control Systems Laboratory, Princeton University, Princeton, NJ, as an Associate Researcher. His main research interest is in the dynamics, controls, and navigation of underwater vehicles. His current research includes multivehicle control, surface independent navigation, and novel actuator designs.

David M. Fratantoni (M'00) received the B.S. degree in ocean engineering from Virginia Polytechnic Institute and State University (Virginia Tech), Blacksburg, in 1990 and the Ph.D. degree in meteorology and physical oceanography from the University of Miami, Coral Gables, FL, in 1996.

He is a Physical Oceanographer at the Woods Hole Oceanographic Institution, Woods Hole, MA. His research interests include observational studies of ocean circulation; investigation of the structure and significance of mesoscale rings; exploration of the relationships between physics and biology on various scales; and development of autonomous instrument platforms, sensors, and observing systems.